European Journal of Cell Biology 100 (2021) 151178

Contents lists available at ScienceDirect

European Journal of Cell Biology

journal homepage: www.elsevier.com/locate/ejcb

Effects of substrate stiffness on mast cell migration

Yi Yu [a], Liu-Jie Ren [b], Xin-Yue Liu [c], Xiao-Bo Gong [d], Wei Yao [a,*]

[a] Shanghai Key Laboratory of Acupuncture Mechanism and Acupoint Function, Department of Aeronautics and Astronautics, Fudan University, No.220 Handan Road, Shanghai, 200433, China
[b] ENT Institute, Eye & ENT Hospital of Fudan University, No.83 Fenyang Road, Shanghai, 200031, China
[c] Shanghai Institute of Applied Mathematics and Mechanics, School of Mechanics and Engineering Science, Shanghai Key Laboratory of Mechanics in Energy Engineering, Shanghai University, Shanghai 200072, China
[d] Key Laboratory of Hydrodynamics (Ministry of Education), Department of Engineering Mechanics, School of Naval Architecture, Ocean and Civil Engineering, Shanghai Jiao Tong University, Shanghai 200240, China

ARTICLE INFO

Keywords:
Mast cells
Migration
Stiffness
Trajectory
Cell morphology

ABSTRACT

Mast cells (MCs) play important roles in multiple pathologies, including fibrosis; however, their behaviors in different extracellular matrix (ECM) environments have not been fully elucidated. Accordingly, in this study, the migration of MCs on substrates with different stiffnesses was investigated using time-lapse video microscopy. Our results showed that MCs could appear in round, spindle, and star-like shapes; spindle-shaped cells accounted for 80–90 % of the total observed cells. The migration speed of round cells was significantly lower than that of cells with other shapes. Interestingly, spindle-shaped MCs migrated in a jiggling and wiggling motion between protrusions. The persistence index of MC migration was slightly higher on stiffer substrates. Moreover, we found that there was an intermediate optimal stiffness at which the migration efficiency was the highest. These findings may help to improve our understanding of MC-induced pathologies and the roles of MC migration in the immune system.

1. Introduction

Mast cells (MCs) are implicated in immune regulation, inflammation, wound healing, and acupuncture analgesia (Ribatti, 2019; Nigrovic, 2017; Zhang et al., 2008). MC migration and recruitment have been reported in various pathologies, including tissue fibrosis, joint diseases, and inflammation of the lungs, intestines, and airways (Nigrovic and Lee, 2007; Legere et al., 2019; Bradding et al., 2006). Moreover, MCs can migrate between different tissues, e.g., from the skin to the draining lymph nodes (Byrne et al., 2008; Wang et al., 1998), from the lungs to the airway smooth muscle (Brightling et al., 2005), and from the jejunum to the spleen (Friend et al., 1998). Numerous studies have focused on chemicals that regulate MC migration owing to their pivotal roles in immediate hypersensitivity and chronic allergic reactions (Okayama and Kawakami, 2006). Furthermore, the effects of the mechanical properties of the extracellular matrix (ECM), which plays important roles in cell migration (Yeung et al., 2005), remain largely unknown.

The role of substrate stiffness in cell migration has been investigated on different cell types, including fibroblasts (Yeung et al., 2005; Lo et al., 2000), cancer cells (McKenzie et al., 2018; DuChez et al., 2019; Bangasser et al., 2017; Wang et al., 2020), and vascular smooth muscle cells (VSMCs) (Isenberg et al., 2009; Wong et al., 2003). When cultured on a substrate with a stiffness gradient, most cells migrate to the stiffer side, a mechanism termed "durotaxis" (Lo et al., 2000). By contrast, when cultured on a substrate with uniform stiffness, the cells move randomly with no directional bias. Moreover, the migration velocity and persistence are stiffness-dependent (Wang et al., 2020; Koser et al., 2016; Lachowski et al., 2017) and closely related to physiological and pathological processes.

Various cell types respond differently to substrate stiffness. Some cells move faster on stiffer substrates, whereas others act in the opposite manner. For example, SKOV3 cells move faster on stiffer substrates; thus, ECM rigidity enhances the metastasis of epithelial ovarian cancer (McKenzie et al., 2018). Additionally, VSMCs show similar stiffness dependence, and this feature may be involved in various vascular diseases, such as atherosclerosis (Isenberg et al., 2009). By contrast, macrophages have been shown to move faster on soft substrates and tend to accumulate in stiffer environments. Therefore, soft tissues exhibit an anti-inflammatory phenotype, whereas stiffer tissues exhibit a

* Corresponding author.
E-mail address: weiyao@fudan.edu.cn (W. Yao).

https://doi.org/10.1016/j.ejcb.2021.151178
Received 21 May 2021; Received in revised form 13 September 2021; Accepted 13 September 2021
Available online 17 September 2021

pro-inflammatory phenotype (Hind et al., 2016; Cougoule et al., 2012). Moreover, the velocity of many cell types exhibits an interesting "biphasic" dependence on ECM stiffness; that is, cells move fastest on an intermediate "optimal stiffness". This feature has been reported in glioma cells (Wang et al., 2020; Marhuenda et al., 2021), neutrophils (Stroka and Aranda-Espinoza, 2009), smooth muscle cells (SMCs) (Peyton and Putnam, 2005), hepatic cells (L02 cells), and hepatocellular carcinoma cells (M3 cells) (Yangben et al., 2013). The non-monotonic relationship between ECM stiffness and cell velocity therefore complicates our understanding of the pathological processes of cancer progression and lung fibrosis and highlights the need to develop smart biomaterials to direct cell migration.

Despite numerous experimental and theoretical studies in other cell types, the influence of substrate stiffness on MC migration has not been extensively studied. (Yang et al. (2018)) cultured MCs on a substrate with two different stiffnesses and a middle gradient zone. Their results showed that MCs tended to gather at the gradient zone. Without quantifying MC migration (e.g., velocity and persistence), it is unclear why MCs prefer the gradient zone. Moreover, numerous studies have demonstrated that tissue fibrosis (e.g., liver cirrhosis (Adolf et al., 2012), myocardial fibrosis (Legere et al., 2019), scleroderma (Saigusa et al., 2018), and fibrotic scars (Hinz, 2009)) is associated with changes in MC density and activation. Therefore, investigations into the influence of substrate stiffness on MC migration characteristics are needed to improve our understanding of the roles of MCs in these pathologies.

Accordingly, in this study, we evaluated the free migration processes of MCs on four substrates with different stiffness using time-lapse video microscopy. MC migration trajectories were identified by self-written MATLAB codes, and various parameters, including velocity, persistence index, and turning angles, were analyzed. Our results show that MCs could appear in round, spindle, and star-like shapes and that the migration speed of round-shaped cells was significantly lower than that of cells with other shapes. Finally, we found that there was an intermediate optimal stiffness at which the migration efficiency was the highest. These results provide important insights into the effects of substrate stiffness on MC migration.

2. Materials and methods

2.1. Cell culture

RBL-2H3 rat basophilic leukemia cells have biological characteristics and functions similar to those of MCs. Therefore, these cells are widely used as a model for studying the biological behaviors of MCs, such as degeneration (Fowlkes et al., 2013) and migration (Jolly et al., 2005; Hou et al., 2020; Marcatti Amarú Maximiano et al., 2017). RBL-2H3 cells (kindly provided by Cell Bank, Chinese Academy of Sciences) were cultured at 37℃ under an atmosphere containing 5% CO_2 in minimum essential medium (Thermo Fisher Scientific, USA) supplemented with 15 % fetal bovine serum, 1% penicillin/streptomycin, and 1% L-glutamine (Gibco, Invitrogen, Grand Island, NY, USA). The cell culture medium was changed every 2–3 days, and cells were passaged during the exponential phase of growth (before the cells reached confluence). Cells were used at passages 4–8.

2.2. Substrate preparation and conjugation

Poly-di-methyl-siloxane (PDMS, w/w; Sylgard 184; Dow-Corning, Midland, MI, USA) is broadly used to fabricate substrates with varying mechanical and geometrical properties for cell culture (Gutekunst et al., 2014; Tzvetkova-Chevolleau et al., 2008) owing to its excellent biocompatibility. PDMS is a mixture of the base and agent. Substrates with different Young's moduli can be obtained by varying their mass ratios. In this experiment, substrates were prepared with 10/30/50:1 base-to-agent ratios. Then, the mixture was settled in a vacuum pump for 1 h at room temperature to eliminate bubbles and transferred to a 6-well plate (3 mL/well) for 1 h to rest. Finally, the mixture was placed in an oven and baked at 75 °C for 6 h and subjected to ultraviolet irradiation for 3 h to obtain substrates with different stiffnesses.

Micro-indentations were performed using atomic force microscopy (AFM; Bruker-Icon) to measure and verify the substrate stiffness. The measurements were performed using silicon nitride AFM cantilevers (PT.PS; Novascan; nominal stiffnesses of 0.03 and 0.12 nN/nm) and polystyrene microspheres (4.5 μm in diameter). During the measurement, PDMS samples were positioned on the optical microscope stage. Indentations were evaluated at random points on the sample surface, with intervals of at least 20 μm, a loading rate of 1 μm/s, and an engaging force of 1 nN. The acquired force-indentation curves were analyzed using Bruker-Nanoscope Analysis software (Bruker) to extract the elastic modulus at each point. For each sample, 16 points were tested. The average moduli of PDMS samples used in this experiment were 83.28 (10:1), 51.25 (30:1), and 29.77 kPa (50:1), respectively, which were comparable to the stiffness range of fibrosis tissue (20–100 kPa) (Wells and Discher, 2008; Goffin et al., 2006; Engler et al., 2008).

Fibronectin coating was carried out after preparation of substrate samples. The substrate was washed three times with phosphate-buffered saline (PBS; pH 7.2; Thermo Fisher Scientific), and 3 mL human plasma fibronectin solution (10 μg/mL; Gibco) was added. The substrate and solution were incubated at 37 °C for 1 h. The solution was then removed, and the coated substrate was rinsed three times with PBS.

2.3. Time-lapse video microscopy

Cells were seeded onto fibronectin-coated PDMS gels or plastic plates (Young's modulus: 10^7 kPa) at a density of 3500 cells/cm^2 to reduce cell-cell contact. Then, the cells were placed into a humidity incubator for 12 h. The supernatants were discarded and replaced with 3 mL fresh culture medium. For imaging, the 6-well plate was fixed on a Stage Top Incubator (Tokai Hit, Japan), and a controller (Tokai Hit) was used to maintain the cell culture atmosphere (37 °C, 5% CO_2, and 95 % humidity). Moreover, an inverted microscope (Ti-E; Nikon, Japan; phase contrast, 10 × 0.3 NA) equipped with a CCD camera (CoolSnap DYNO Scientific, USA) was used for cell imaging, and NIS-Element software was used to control the imaging process. Imaging was carried out for 2 h, and one frame was recorded every 2 min. Before long-term observation, the cells were precultured in a Stage Top Incubator for 1 h. For each stiffness group, the experiment was repeated more than three times.

2.4. Image processing

In total, of 61 frames, with approximately 80–100 cells per frame, were captured for each group (frame time interval, $\Delta T = 2$ min). Then, the cell migration trajectory was extracted from the frames (Fig. 1A). For each frame, the cell edges were manually marked, and the cell centers were automatically calculated using a self-written code in MATLAB. Automatic cell matching between two neighboring frames was fulfilled by searching the nearest cells. However, for cell i at a certain frame, if no cells were found within a distance of 25 μm in the next frame, typically because the cell disengaged from the substrate and moved away, then the cell was excluded. The cell matching process was monitored manually and corrected if necessary.

Additionally, for each frame, cell shapes were analyzed (Fig. 1B). The cell shape was described by the radius of cell (θ), determined by the distance between points on the cell edge and cell center. Briefly, the cells were classified as: "round" if $R(\theta)$ was flat, "spindle" if $R(\theta)$ had one or two peaks, and "star-like" if $R(\theta)$ had three or more peaks. This shape classification based on the number of protrusions was very intuitive; however, we should note that this classification method was specifically designed for RBL-2H3 cells and may therefore be limited to studies using this cell type.

Because cells may change shapes over time, for each cell i, there is a list of $F = 61$ cell shapes ($Shape(i,k)$, where $k = 1, 2, \ldots, F$). For each cell

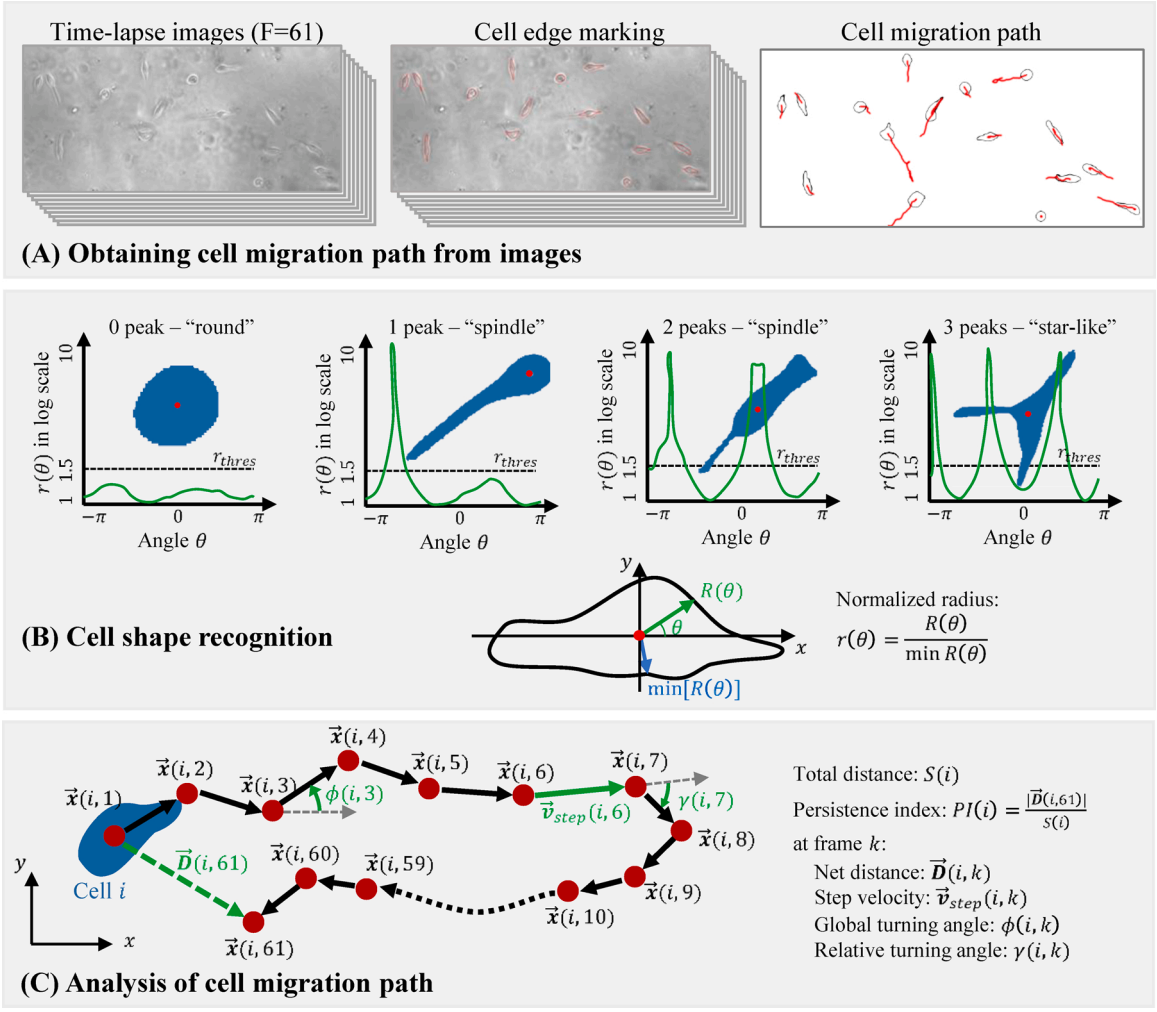

Fig. 1. Image processing and analysis of cell migration properties. (A) Obtaining cell migration trajectory from images. The picture on the left is of time-lapse images from NIS-Element software; that in the middle shows cell edge marking; and that on the right shows the cell migration trajectory. (B) Cell shape recognition. The top four graphs show different shapes. The lower graph shows how the normalized radius was obtained. (C) Analysis of cell migration path.

i, the "dominant" shape, *DShape*(*i*), was determined by the shape with the most frequent occurrence in all frames.

2.5. Analysis of cell migration properties

Fig. 1C shows an intuitive demonstration of the trajectory analysis. The migration trajectory of a certain cell *i* is described as a list of locations, defined as $\vec{x}(i,k) = [x,y](i,k), k = 1,2,\ldots,F$, corresponding to time 0, 2, …, 120 min. For each path, the total distance is defined as

$$S(i) = \sum_{k=1}^{F-1} |\vec{x}(i,k+1) - \vec{x}(i,k)| \quad (1)$$

and the net distance at frame *k* is defined as $\vec{D}(i,k) = \vec{x}(i,k) - \vec{x}(i,1)$. Then the mean square distance (MSD) is calculated as

$$MSD(k) = \sum_{i=1}^{n} \left|\vec{D}(i,k)\right|^2, \quad (2)$$

where *n* is the number of cells. The step velocity (for cell *i* at frame *k*) is

$$\vec{v}_{step}(i,k) = \frac{1}{\Delta T}(\vec{x}(i,k+1) - \vec{x}(i,k)) \quad (3)$$

and the cell velocity is determined by

$$v(i) = \frac{1}{F-1}\sum_{k}^{F-1} |\vec{v}_{step}(i,k)| = \frac{S(i)}{(F-1)\Delta T}. \quad (4)$$

The cell persistence is evaluated by the "persistent index" (*PI*), defined as

$$PI(i) = \frac{\left|\vec{D}(i,F)\right|}{S(i)} \in [0,1] \quad (5)$$

As *PI* approaches 1, the cell tends to keep its direction and moves along a straight line.

The global turning angle of cell migration is calculated as

$$\phi(i,k) = \tan^{-1}\left(\frac{\vec{v}_{step}(i,k)\cdot\vec{n}_y}{\vec{v}_{step}(i,k)\cdot\vec{n}_x}\right) \quad (6)$$

where $\vec{n}_x$ and $\vec{n}_y$ are normal vectors pointing to the *x* and *y* axes, respectively. The relative turning angle is defined by

$$\gamma(i,k) = \cos^{-1}\left(\frac{\vec{v}_{step}(i,k)\cdot\vec{v}_{step}(i,k+1)}{\left|\vec{v}_{step}(i,k)\right|\cdot\left|\vec{v}_{step}(i,k+1)\right|}\right) \quad (7)$$

2.6. Statistics

Data were divided into four groups. Mean values and variance were calculated and expressed as means ± standard errors. One-way analysis of variance (ANOVA) was used to analyze the mean values and variances of cell velocity and the persistence index, whereas Tukey's post-hoc test was used for comparisons among multiple groups. All statistical analyses were performed using MATLAB statistics and machine learning toolbox (MATLAB 2020a, Mathworks). Results with *P* values less than 0.05 were considered significant.

3. Results

3.1. Cell shapes and velocity

RBL-2H3 cells exhibit different shapes when cultured on substrates. According to the number of protrusions, MCs can be classified as "round", "spindle", or "star-like" (Fig. 1B). Round-shaped cells had no protrusions, spindle-shaped cells had one or two protrusions, and star-like cells had three or more protrusions (Fig. 2A). For a single cell, the cells shape could vary over time. For example, cells initially exhibiting a round shape could become deformed into spindle-shaped cells, and vice versa. For consistency, we labelled each cell with the shape that was maintained most of the time. Table 1 shows the percentages of the three cell types on the four substrates. Spindle-shaped cells accounted for the majority of cells ($\geq$ 80 %) on all substrates and were the most common cell type (90 %) on the 51.25 kPa substrate.

The velocity of RBL-2H3 cells was shape-dependent. Fig. 2B shows the velocities of the three cell types on all substrates. The mean velocities for round, spindle-shaped, and star-like cells were 0.47 ± 0.03, 1.03 ± 0.02, and 0.91 ± 0.10 μm/min, respectively. Thus, these findings showed that the velocity of round cells was significantly lower than that of the other two cell types ($p < 1 \times 10^{-6}$).

3.2. Unbiased migration of RBL-2H3 cells

Single-cell migration is thought to follow random walk pattern, which is unbiased when the substrate is uniform and biased when there is a chemical/mechanical gradient (Codling et al., 2008). Unbiased cell migration fits into the persistent random walk (PRW) model, where persistence means that the cell "remembers" and maintains the moving direction with a certain probability. For a long-term unbiased two-dimensional (2D) random walk (Andreanov and Grebenkov, 2012), the cell distribution is similar to that of free diffusion, and the *MSD* is proportional to time *t*:

Table 1
Proportions of round, spindle, and star-like cells on substrates with different stiffnesses.

Group	Cell number	Round	Spindle	Star-like
10^7 kPa	98	10 (10.21 %)	83 (84.69 %)	5 (5.10 %)
83.28 kPa	103	19 (18.45 %)	82 (79.61 %)	2 (1.94 %)
51.25 kPa	100	2 (2.00 %)	90 (90.00 %)	8 (8.00 %)
29.77 kPa	95	14 (14.74 %)	79 (83.16 %)	2 (2.10 %)
Total	396	45 (11.35 %)	334 (84.37 %)	17 (4.28 %)

$$MSD(t) = 2Dt \tag{8}$$

where *D* is the diffusion coefficient. Fig. 3A and B gives the $MSD - t$ curves for RBL-2H3 cells on four substrates. Because the *MSD* - *t* curves showed a good linear correlation, we calculated the diffusion coefficient *D* for all groups using the least-squares method for linear fitting. The *D* values of cells on 51.25 kPa substrate were 3.05 and 3.36 μm^2/min for all cell shapes and spindle-shaped cells, respectively.

To further verify that the cell migration was unbiased, the global turning angles $\phi(i,k)$ were analyzed, and the distributions are plotted in Fig. 3C and D. The angle distributions were relatively uniform with no global bias.

3.3. Influence of substrate stiffness

The MSD curves (Fig. 3) showed that the cells migrated fastest on the 51.25 kPa substrate. Thus, the influence of substrate stiffness was further investigated to determine cell velocity and persistence. Fig. 4A and B show the relationship of cell velocity with substrate stiffness. The cell velocity was highest on the 51.25 kPa substrate (1.11 and 1.14 μm/min for all cell types and spindle-shaped cells, respectively), which was significantly different from that of cells cultured on stiffer or softer substrates. Thus, we concluded that 51.25 kPa was close to the "optimal stiffness".

Stiffness may also affect persistence (Ng et al., 2012). Fig. 4C and D shows the direction PI of cells on substrates with different stiffnesses. For most cells, the PI values were below 0.2. Thus, the PI increased slightly as the ECM stiffness decreased; however, no significant differences were observed among groups. For all three cell types (Fig. 4C), the PI values (means ± standard errors of the means) were 0.11 ± 0.01 and 0.16 ± 0.02 on the 10^7 kPa and 29.77 kPa substrates, respectively. Similar results were observed for spindle cells only (Fig. 4D).

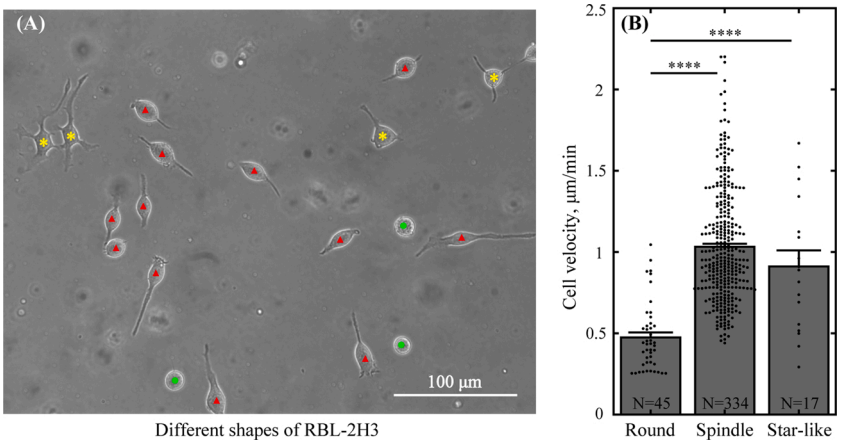

Different shapes of RBL-2H3

Fig. 2. Different shapes of RBL-2H3 cells and corresponding velocities. (A) Cells labelled with '●', '▲', and '*' are classified as round, spindle, and star-like cells, respectively. Some cells were not labeled because they were excluded from analysis owing to blurry boundaries or detachment from the substrate. (B) Velocities of the round, spindle, and star-like cells. **** $p < 0.0001$. N is the cell number.

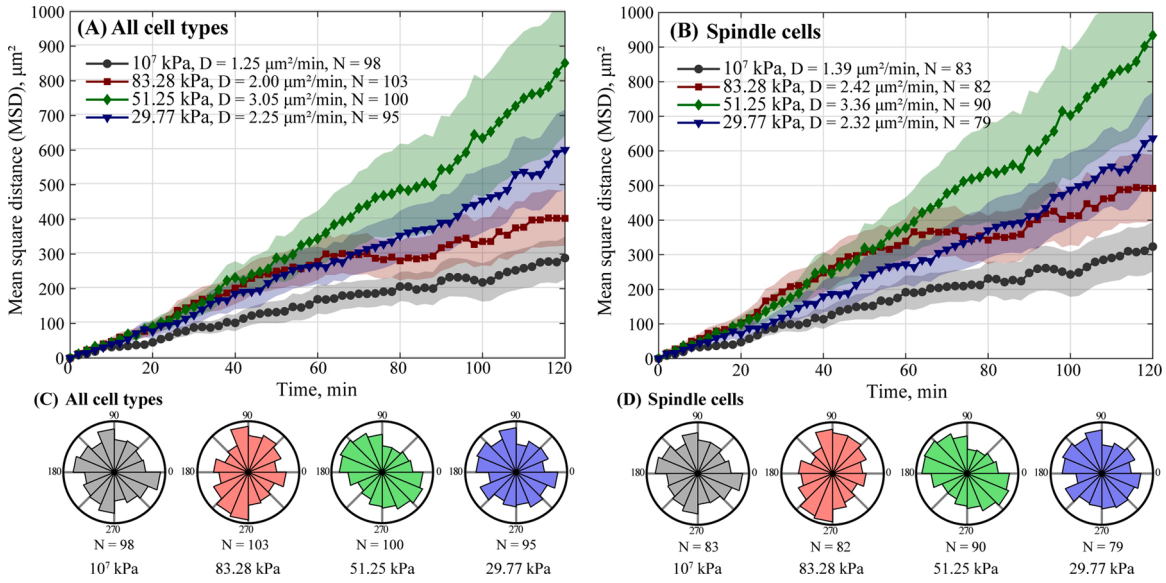

Fig. 3. MSD – t curves and global turning angle of RBL-2H3 cells on substrates with four different stiffnesses. (A, B) MSD – t curves. Lines with markers show the MSD curves, and shadows show the corresponding standard deviations. The diffusion coefficients (D) were calculated using a linear fit of $MSD = 2Dt$. N is the cell number. (C, D) Global turning angle. (A, C) All cells (round, spindle, and star-like) were counted. (B, D) Only spindle-shaped cells were counted.

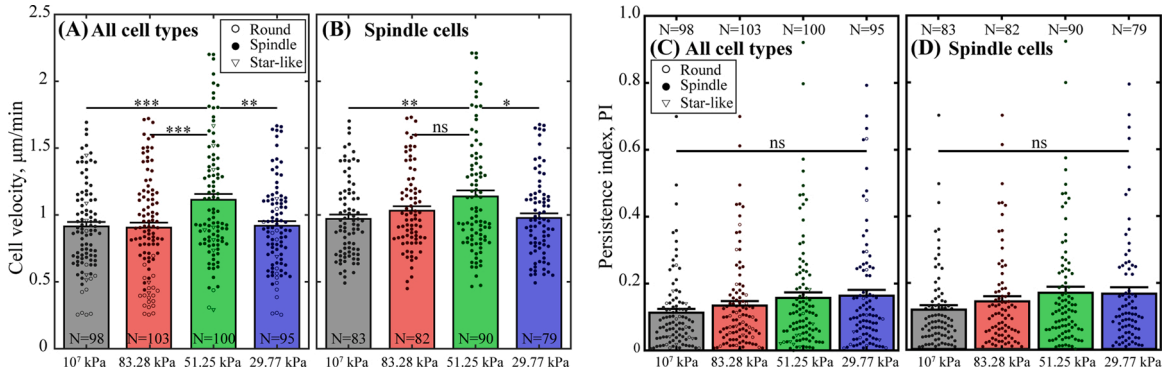

Fig. 4. Velocity and direction persistence index (PI) of RBL-2H3 cells on substrates with different stiffnesses. (A) Velocities of all cell types. The markers represent data for each cell, with '○' for round cells, '●' for spindle-shaped cells, and '▽' for star-like cells. (B) Velocities of spindle-shaped cells only. N is the cell number. (C) PI values of all cell types. (D) PI values of spindle-shaped cells only. N is the cell number. * $p < 0.05$; ** $p < 0.01$; *** $p < 0.001$; ns, not significant.

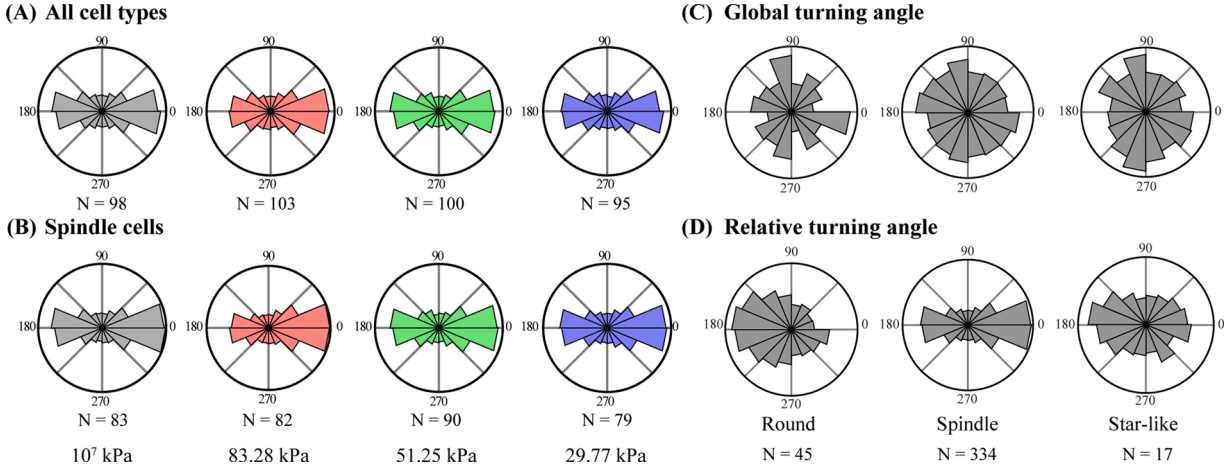

Fig. 5. Turning angles of RBL-2H3 cells on substrates with different stiffnesses. (A, B) Relative turning angles for all three cell types (round, spindle, and star-like) and for spindle-shaped cells only. (C, D) Global and relative turning angles of round, spindle, and star-like cells. N is the cell number.

3.4. Relative turning angles

Fig. 5A and B show the relative turning angle $\gamma(i,k)$ of RBL-2H3 cells. The results showed that RBL-2H3 cells had two frequent turning angles, 0 ° and 180 °, during migration. Thus, the cells had a good chance of move forwards (0 °) or backwards (180 °).

Since the pattern of the relative turning angles differed from that of the global turning angles, we further compared both the relative and global turning angles of the three cell shapes. Fig. 5C and D shows the global and relative turning angles of round, spindle-shaped, and star-like cells. The global turning angles of the three cell shapes were almost uniformly distributed, indicating no global bias. Moreover, the distributions of relative turning angles varied dramatically. The round cells had a relatively higher probability of moving backward (180 °), indicating that round cells tended to jiggle and wiggle around in place since the cell velocity was slow. Spindle-shaped cells tended to move on a straight line, but also had a significant chance of moving backward. Considering the large proportion of spindle-shaped cells, this type of motion was the most common motion for RBL-2H3 cells (Fig. 5A, B). Compared with that of spindle-shaped cells, the relative turning angle distribution of star-like cells was less polarized, indicating a higher probability of turning left or right for star-like cells when moving forward or backward. The differences in relative turning angles are not surprising considering that cell migration largely depends on protrusions, which determine the cell shape.

4. Discussion

4.1. Optimal stiffness for cell migration

Substrate stiffness is known to affect cell migration speed. Indeed, many types of cells have faster speeds or migration efficiencies on rigid substrates. However, stiffness-velocity curves for some cells, such as U251 glioma cells (Bangasser et al., 2017), neutrophils (Stroka and Aranda-Espinoza, 2009), and SMCs (Peyton and Putnam, 2005), exhibit biphasic properties. In this study, the MSD and velocity of MCs on the 51.25 kPa substrate were significantly higher than those of the other three groups, indicating that the migration of MCs had similar biphasic properties on the "optimal stiffness" substrate. From the perspective of the PRW model (Prahl et al., 2020), the high migration efficiency of MCs could be related to two specific factors. First, the cell speed conformed to the biphasic distribution, and second, the cell migration direction persistence was slightly better on softer substrates or substrates that were close to the optimum stiffness.

This issue may be related to the dynamic mechanism of cell migration. Assuming the substrate as an elastic material, Ji et al. introduced a "motility factor" to represent the ratio of the driving force to cell movement resistance (Zhong and Ji, 2013). Their simulation results revealed that the "motility factor" changed with the substrate stiffness and had biphasic properties. Cells cannot migrate effectively when the substrate is too soft to form stable protrusions attaching to the substrate. By contrast, when the substrate stiffness is too high, the protrusions on the trailing edge become tight, resulting in excessive cell migration resistance, which is no conducive to the efficient migration of cells.

4.2. Cell shape and migration speed

In this study, we found that round MCs were significantly slower than spindle-shaped and star-like cells. Round cells exhibit insufficient connections with the substrate and spread more on stiffer substrates, with broader lamellipodia (DuChez et al., 2019; Ulrich et al., 2009). Moreover, cell shape has been shown to be related to contractility (Lemmon and Romer, 2010). The traction force is generally considered to be the sum of multiple protrusions forces, and the protrusion force is positively correlated with the distance between the protrusion and the cell center. Therefore, cells with larger areas generally have larger traction forces. In this study, the length of spindle-shaped cells in the spreading direction was generally longer than the diameter of round-shaped cells.

Furthermore, we observed differences in the relative turning angles of the three cell types, suggesting relationships between protrusions and cell migration. Round cells had no obvious protrusions around the cell boundary. Therefore, whenever the cell attempted to move in any direction, it was pulled back, resulting in a jiggling and wiggling motion. Spindle-shaped cells primarily had two protrusions distributed on opposite sides of the cell; therefore, cell movement tended to be in the direction of the cell polar axis (0 ° or 180 °). Finally, star-like cells had more than two protrusions, and the relative turning angles were distributed more evenly.

Califano discussed the interplay among substrate stiffness, cell area, and cell contractility (i.e., the dynamics of cell migration) (Califano and Reinhart-King, 2010). We proposed a similar philosophy (Fig. 6A). In our analysis of the relationships among substrate stiffness, cell shape, and cell migration efficiency, we found that under the "optimal stiffness", the slowest moving round cells accounted for the lowest proportion of cells; thus, the average cell speed may be affected. However, because the total number of MCs was low, it is still unclear whether the substrate stiffness may significantly affect the proportion of round cells. Therefore, we excluded round cells and only investigated spindle-shaped cells, which had the highest proportion. The "optimal stiffness" phenomenon still existed when only spindle-shaped cells were assessed. Consequently, the mechanism through which substrate stiffness affected MC migration may also be involved in the direct interplay.

4.3. Cell velocity, adhesion, and substrate stiffness

Cell migration, cell-substrate adhesion, and substrate stiffness are closely related. Cell velocity may also exhibit biphasic behaviors when cell-substrate adhesion varies. For example, glioma cells exhibit the highest velocity when the expression of CD44, a protein related to cell adhesion, is moderate, and better outcomes in humans and experimental mouse models are observed when CD44 expression is higher or lower (Klank et al., 2017). By contrast, the relationship between substrate stiffness and cell-substrate adhesion is quite clear: a stiffer substrate enhances adhesion, as manifested by a larger spreading area (Lo et al., 2000) and cell-substrate interaction stress (Bollmann et al., 2015). Therefore, this is not surprising that the velocity of glioma cells also shows biphasic dependence on substrate stiffness (Wang et al., 2020; Klank et al., 2017).

Numerous numerical models have been developed to elucidate the influence of the cell-substrate interaction on cell migration. The biphasic behaviors of cell velocity have been demonstrated in different models by DiMilla et al. (1991), Lin (2010), Zhong and Ji (2013), and Pathak (2018). Despite different assumptions and study approaches, all of these models indicate that cell migration is enhanced when the cell-substrate adhesion is neither too strong nor too weak. If too weak, the traction force is small, whereas if too strong, the traction force stops the cell from moving forward.

In this study, a minimal one-dimensional (1D) centroid model was introduced to simulate substrate stiffness-related cell migration. We found that the focal adhesion (FA) stability (expressed by the activation probability in our model) was crucial for cell migration (Fig. 6D, E). Additionally, the "optimal stiffness" may be related to the "optimal activation probability" or "optimal stability" of FAs. If the FAs attached to the substrate too strongly, then the forces exerted by FAs tended to cancel each other out; by contrast, if the FAs were unstable, then the driving force was insufficient.

4.4. 1D centroid model for cell migration

Because MCs are mostly spindle-shaped cells and mainly move along the long axis, a 1D centroid model was introduced to study the dynamics

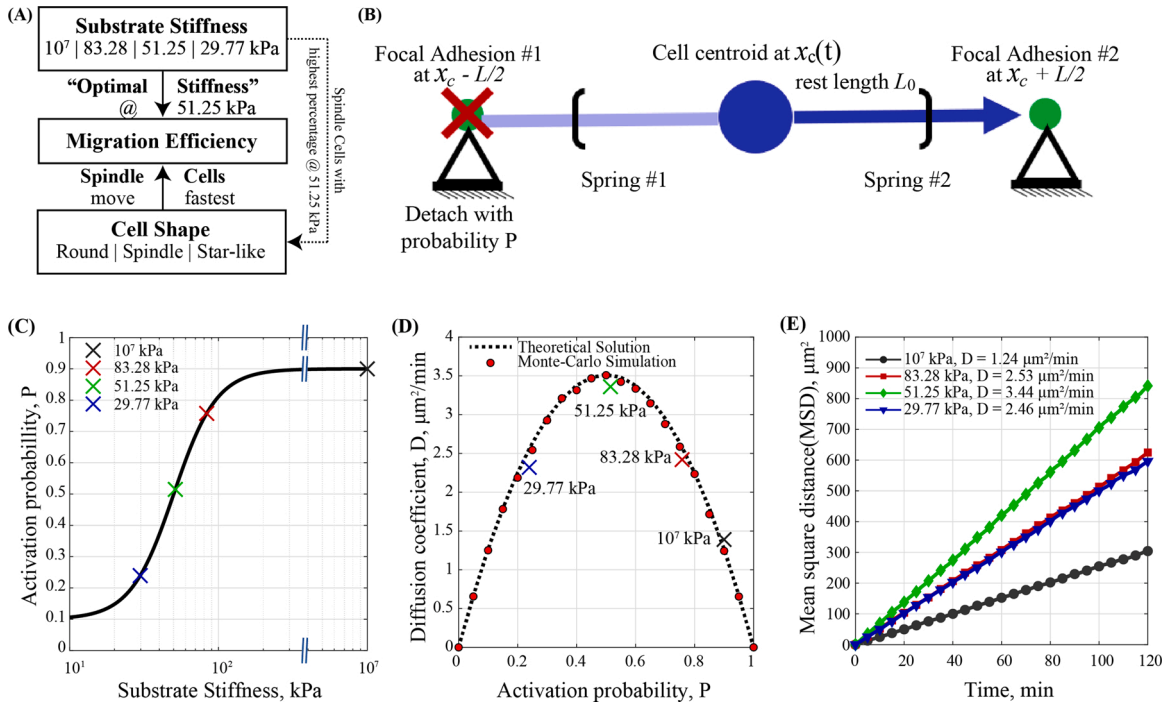

Fig. 6. Intrinsic mechanism and mathematical model of MC migration. (A) Proposed possible interplay among substrate stiffness, cell shape, and migration efficiency in MCs. (B) Sketch of the 1D Spring-Centroid model. (C) The assumed probability of FA activation on substrates with different stiffnesses. The cross markers indicate the fitted results for the same stiffnesses used in our experiments. (D) Relationships between the FA activation probability and the diffusion coefficient. The dotted lines are theoretical results, the dots are from Monte-Carlo simulations, and the cross markers indicate the diffusion coefficient calculated from our experimental results. (E) MSD – t curves for RBL-2H3 cells on substrates with four different stiffnesses. Curves were obtained by Monte-Carlo simulation.

of MC migration (Fig. 6B). The cell was described as a centroid agent located at x_c, with a length of $L = 20\ \mu m$. The cell had two FAs at its edges, and each connected the centroid with a spring (with a spring constant α) representing cytoskeleton links. The FA was either activated or deactivated, as expressed by the activate function ϕ_i. If $\phi_i = 1$, the FA was activated and would exert a force on the centroid. According to Hooke's law, the force is $f = \alpha\left(\frac{L}{2} - L_0\right)$. Here L_0 (assumed to be 6.25 μm in our model) is the rest length of the spring. Otherwise, if $\phi_i = 0$, the FA was deactivated, and no force was applied to the centroid. The centroid moves under the summation of FA forces, whose dynamics can be modeled as (Dallon et al., 2013)

$$\mu\frac{dx_c}{dt} = \sum_{i=1}^{n=2} -\alpha(|x_c - x_i| - L_0)\frac{x_c - x_i}{|x_c - x_i|}\phi_i \tag{8}$$

where x_i is the location of the FA, satisfying that $x_1 = x_c - L/2$ and $x_2 = x_c + L/2$. μ is the drag coefficient. Considering that the response of cell force releasing typically occurs within a few seconds (Chan and Odde, 2008), we assumed that the cell centroid could move 'immediately' to its equilibrium position, such that

$$(x_c - x_1 - L_0)\phi_1 = (x_2 - x_c - L_0)\phi_2 \tag{9}$$

Typically, if $\phi_1 = \phi_2 = 0$, no force was applied to the centroid; thus, the cell maintained its original position. Otherwise, the cell moved to $x_c = \frac{\phi_1(x_1 + L_0) + \phi_2(x_2 - L_0)}{\phi_1 + \phi_2}$ according to the equilibrium equation.

A Monte-Carlo procedure was introduced to simulate the randomness of cell migration. The cell migration process was divided into multiple Monte-Carlo steps (MCSs). At each step, the two FAs at the edges were activated with a probability P, and the cell then moved according to the equilibrium equation. The simple rule was repeated at each MCS, and the cell trajectory was recorded. One MCS corresponded to approximately 1 min because the feature time of FA attachment and detachment has been reported to be approximately 20–100 s (Dallon et al., 2013). In total, 10,000 cells for 120 MCSs were simulated.

The cell migration in our model was controlled by FA activations, in which the activation probability P is a crucial parameter. The substrate is thought to modulate the formation and enzymolysis of FAs. On stiffer substrates, FAs are more stable, with a lower detach rate (Pelham and Wang, 1997). Yang et al. also reported that MCs attached more firmly on stiffer substrates (Yang et al., 2018). Therefore, the activation probability P should be positively correlated with the substrate stiffness E. We assumed that

$$P = P_{\min} + \frac{P_{\max} - P_{\min}}{1 + e^{-\beta(\ln E - \ln E_0)}} \tag{10}$$

where E_0 is the critical Young's modulus. $P_{\max}$, $P_{\min}$, and β are control parameters. The relationship between P and E is plotted in Fig. 6C ($E_0 = 50\ kPa$, $P_{\max} = 0.9$, $P_{\min} = 0.1$, and $\beta = 3$). Notably, the "optimal stiffness" differs among cell types. The values of these parameters were determined such that the simulation results fitted those from our experiments.

Within each MCS, the cell tended to stay still with a probability of $P^2 + (1-P)^2$ (when $\phi_1 = \phi_2 = 1$ or $\phi_1 = \phi_2 = 0$) and to move left or right for a distance of $\frac{L}{2} - L_0$ with a probability of $2P(1-P)$. Thus, cell migration was a simple random walk and yielded the diffusion equation, which was theoretically derived as $D = P(1-P)\left(\frac{L}{2} - L_0\right)^2$ (Codling, 2003). Fig. 6D shows the relationship between the diffusion coefficient D and the activation probability P. The Monte-Carlo simulation results were consistent with the theoretical equation. The diffusion coefficient peaked at $P = 0.5$. The cross markers indicated the relationship between D from the experimental results (Fig. 3B) and the assumed activation probability P according to Eq. (10). As a verification, Fig. 6E shows the simulated MSD curves for cell migration on substrates of the same stiffnesses used in our experimental settings. The curves were very similar to those in Fig. 3B.

4.5. Relevance of MC migration

Novikova et al. assumed that cell durotaxis is related to the faster cell velocity on stiffer substrates (Novikova et al., 2017). To verify this hypothesis, they simulated cell migration on a 2D substrate with a stiffness gradient. The simulation showed that when a cell travels from the softer side to the stiffer side, its velocity increases and the cell moves further to the stiffer side, resulting in the durotaxis phenomenon. Similarly, if the cell velocity has an "optimal stiffness", as found in this study, the cell velocity will increase when the cell approaches the optimal stiffness, whether from the stiffer side or from the softer side. As a result, cells tend to accumulate at the optimal stiffness area, as is reported by (Yang et al. (2018)).

The MC density is increased in many pathologies involving tissue fibrosis (Terada and Matsunaga, 2000; Iamaroon et al., 2003). Such increases may be caused by migration of MC precursors from the bone marrow followed by local maturation, local proliferation of resident MCs, and migration of MCs from adjacent tissues. MCs act as effector cells and produce mediators that regulate the fibrotic process. MCs have been shown to promote fibrosis in liver cirrhosis (Adolf et al., 2012) and myocardial fibrosis (Legere et al., 2019). However, MCs can also suppress fibrosis, particularly in the process of myocardial fibrosis (Legere et al., 2019). Therefore, the roles of MCs in fibrosis remains controversial.

Increased matrix stiffness is not only a pathological consequence of fibrosis but also conversely affects pathological progression (Chen et al., 2019). The mechanical properties of the ECM (stress or strain) induce MC degranulation (Fowlkes et al., 2013); however, the mechanical effects (e.g., fibrosis-induced changes in stiffness) on other MC phenotypes, such as proliferation, maturation, and migration, are not fully understood. In this study, we found that ECM stiffness may also influence MC migration. Thus, these results provided important insights into the impact of MCs on fibrosis-related pathologies and may help to establish novel therapeutic strategies.

4.6. Limitations and future research perspectives

Our analysis in this study was conducted based on 2D culturing and monitoring of MCs. However, cell migration on 2D and three-dimensional (3D) substrates may differ significantly. Thus, further studies are needed to assess MC migration in 3D substrates. Furthermore, more detailed analyses of the relationships between MC shape and adhesion properties (such as cell-substrate traction force) are needed.

5. Conclusion

The MC migration characteristics on four substrates with different stiffnesses were evaluated in this study using real-time tracking and analysis of cell trajectories. We analyzed cell shape, velocity, and persistence and assessed the relationships of these characteristics with substrate stiffness. Our findings revealed that there were three MC shapes (round, spindle, and star-like), with spindle-shaped cells accounting for 80–90 % of the total cells. Additionally, the migration speed of round cells was significantly lower than those of spindle and star-like cells. From this analysis, we identified the "optimal stiffness" of the substrate, which resulted in a higher velocity and better persistence.

Overall, our findings showed that cell-substrate interactions modulate not only the degranulation of MCs but also their migration. The dependence of MC migration on substrate stiffness may be an essential feature of MC-induced pathologies, such as fibrosis of multiple tissues and organs.

CRediT authorship contribution statement

Yi Yu: Methodology, Formal analysis, Resources, Visualization, Writing – original draft. **Liu-Jie Ren:** Methodology, Software, Writing – review & editing. **Xin-Yue Liu:** Methodology, Writing – review & editing. **Xiao-Bo Gong:** Methodology, Writing – review & editing. **Wei Yao:** Conceptualization, Writing – review & editing, Supervision, Funding acquisition.

Declaration of Competing Interest

The authors report no declarations of interest.

Acknowledgements

We thank Dr. Hua-Xiong Huang (York University) for beneficial suggestions and enthusiastic help with the writing of this manuscript. This research was funded by National Natural Science Foundation of China (grant number: 12172092, 82174488) and Shanghai Key Laboratory of Acupuncture Mechanism and Acupoint Function (grant number: 21DZ2271800).

References

Adolf, S., Millonig, G., Seitz, H.K., et al., 2012. Systemic mastocytosis: a rare case of increased liver stiffness. Case Reports Hepatol.
Andreanov, A., Grebenkov, D.S., 2012. Time-averaged MSD of brownian motion. J. Stat. Mech. Theory Exp. 7, P07001.
Bangasser, B.L., Shamsan, G.A., Chan, C.E., et al., 2017. Shifting the optimal stiffness for cell migration. Nat. Commun. 8 (1), 1–10.
Bollmann, L., Koser, D.E., Shahapure, R., et al., 2015. Microglia mechanics: immune activation alters traction forces and durotaxis. Front. Cell. Neurosci. 9, 363.
Bradding, P., Walls, A.F., Holgate, S.T., 2006. The role of the mast cell in the pathophysiology of asthma. J. Allergy Clin. Immunol. Pract. 117 (6), 1277–1284.
Brightling, C.E., Ammit, A.J., Kaur, D., et al., 2005. The CXCL10/CXCR3 axis mediates human lung mast cell migration to asthmatic airway smooth muscle. Am. J. Respir. Crit. Care Med. 171 (10), 1103–1108.
Byrne, S.N., Limón-Flores, A.Y., Ullrich, S.E., 2008. Mast cell migration from the skin to the draining lymph nodes upon ultraviolet irradiation represents a key step in the induction of immune suppression. J. Immunol. 180 (7), 4648–4655.
Califano, J.P., Reinhart-King, C.A., 2010. Substrate stiffness and cell area predict cellular traction stresses in single cells and cells in contact. Cell. Mol. Bioeng. 3 (1), 68–75.
Chan, C.E., Odde, D.J., 2008. Traction dynamics of filopodia on compliant substrates. Science 322 (5908), 1687–1691.
Chen, G., Xia, B., Fu, Q., et al., 2019. Matrix mechanics as regulatory factors and therapeutic targets in hepatic fibrosis. Int. J. Biol. Sci. 15 (12), 2509.
Codling, E.A., 2003. Biased Random Walks in Biology. Doctoral Dissertation. University of Leeds, pp. 6–7. Chapter 1.
Codling, E.A., Plank, M.J., Benhamou, S., 2008. Random walk models in biology. J. R. Soc. Interface 5 (25), 813–834.
Cougoule, C., Van Goethem, E., Le Cabec, V., et al., 2012. Blood leukocytes and macrophages of various phenotypes have distinct abilities to form podosomes and to migrate in 3D environments. Eur. J. Cell Biol. 91 (11–12), 938–949.
Dallon, J.C., Scott, M., Smith, W.V., 2013. A force based model of individual cell migration with discrete attachment sites and random switching terms. J. Biomech. Eng.-Tasme 135 (7).
DiMilla, P.A., Barbee, K., Lauffenburger, D.A., 1991. Mathematical model for the effects of adhesion and mechanics on cell migration speed. Biophys. J. 60 (1), 15–37.
DuChez, B.J., Doyle, A.D., Dimitriadis, E.K., et al., 2019. Durotaxis by human cancer cells. Biophys. J. 116 (4), 670–683.
Engler, A.J., Carag-Krieger, C., Johnson, C.P., et al., 2008. Embryonic cardiomyocytes beat best on a matrix with heart-like elasticity: scar-like rigidity inhibits beating. J. Cell. Sci. 121 (22), 3794–3802.
Fowlkes, V., Wilson, C.G., Carver, W., et al., 2013. Mechanical loading promotes mast cell degranulation via RGD-integrin dependent pathways. J. Biomech. 46 (4), 788–795.
Friend, D.S., Gurish, M.F., Hunt, J., et al., 1998. Fate of jejunal mast cells in mice infected with Trichinella spiralis. FASEB (Fed. Am. Soc. Exp. Biol.) J 12, A894.
Goffin, J.M., Pittet, P., Csucs, G., et al., 2006. Focal adhesion size controls tension-dependent recruitment of α-smooth muscle actin to stress fibers. J. Cell Biol. 172 (2), 259–268.
Gutekunst, S.B., Grabosch, C., Kovalev, A., et al., 2014. Influence of the PDMS substrate stiffness on the adhesion of Acanthamoeba castellanii. Beilstein J. Nanotechnol. 5 (1), 1393–1398.
Hind, L.E., Lurier, E.B., Dembo, M., et al., 2016. Effect of M1–M2 polarization on the motility and traction stresses of primary human macrophages. Cell. Mol. Bioeng. 9 (3), 455–465.
Hinz, B., 2009. Tissue stiffness, latent TGF-β1 activation, and mechanical signal transduction: implications for the pathogenesis and treatment of fibrosis. Curr. Rheumatol. Rep. 11 (2), 120.
Hou, Y.B., Zhang, L.N., Wang, H.N., et al., 2020. The antipsychotic drug pimozide inhibits IgE-mediated mast cell degranulation and migration. Int. Immunopharmacol. 84, 106500.

Iamaroon, A., Pongsiriwet, S., Jittidecharaks, S., et al., 2003. Increase of mast cells and tumor angiogenesis in oral squamous cell carcinoma. J. Oral Pathol. Med. 32 (4), 195–199.
Isenberg, B.C., DiMilla, P.A., Walker, M., et al., 2009. Vascular smooth muscle cell durotaxis depends on substrate stiffness gradient strength. Biophys. J. 97 (5), 1313–1322.
Jolly, P.S., Bektas, M., Watterson, K.R., et al., 2005. Expression of SphK1 impairs degranulation and motility of RBL-2H3 mast cells by desensitizing S1P receptors. Blood 105 (12), 4736–4742.
Klank, R.L., Grunke, S.A., Bangasser, B.L., et al., 2017. Biphasic dependence of glioma survival and cell migration on CD44 expression level. Cell Rep. 18 (1), 23–31.
Koser, D.E., Thompson, A.J., Foster, S.K., et al., 2016. Mechanosensing is critical for axon growth in the developing brain. Nat. Neurosci. 19 (12), 1592–1598.
Lachowski, D., Cortes, E., Pink, D., et al., 2017. Substrate rigidity controls activation and durotaxis in pancreatic stellate cells. Sci. Rep.-UK 7 (1), 1–12.
Legere, S.A., Haidl, I.D., Légaré, J.F., et al., 2019. Mast cells in cardiac fibrosis: new insights suggest opportunities for intervention. Front. Immunol. 10, 580.
Lemmon, C.A., Romer, L.H., 2010. A predictive model of cell traction forces based on cell geometry. Biophys. J. 99 (9), L78–80.
Lin, Y., 2010. A model of cell motility leading to biphasic dependence of transport speed on adhesive strength. J. Mech. Phys. Solids 58 (4), 502–514.
Lo, C.M., Wang, H.B., Dembo, M., et al., 2000. Cell movement is guided by the rigidity of the substrate. Biophys. J. 79 (1), 144–152.
Marcatti Amarú Maximiano, W., Marino Mazucato, V., Tambasco de Oliveira, P., et al., 2017. Nanotextured titanium surfaces stimulate spreading, migration, and growth of rat mast cells. J. Biomed. Mater. Res. A 105 (8), 2150–2161.
Marhuenda, E., Fabre, C., Zhang, C., et al., 2021. Glioma stem cells invasive phenotype at optimal stiffness is driven by MGAT5 dependent mechanosensing. J. Exp. Clin. Cancer Res. 40 (1), 1–4.
McKenzie, A.J., Hicks, S.R., Svec, K.V., et al., 2018. The mechanical microenvironment regulates ovarian cancer cell morphology, migration, and spheroid disaggregation. Sci. Rep.-UK 8 (1), 1–20.
Ng, M.R., Besser, A., Danuser, G., et al., 2012. Substrate stiffness regulates cadherin-dependent collective migration through myosin-II contractility. J. Cell Biol. 199 (3), 545–563.
Nigrovic, P.A., 2017. Mast Cells. Kelley and Firestein's Textbook of Rheumatology. Elsevier, pp. 250–263.
Nigrovic, P.A., Lee, D.M., 2007. Synovial mast cells: role in acute and chronic arthritis. Immunol. Rev. 217 (1), 19–37.
Novikova, E.A., Raab, M., Discher, D.E., et al., 2017. Persistence-driven durotaxis: generic, directed motility in rigidity gradients. Phys. Rev. Lett. 118 (7), 078103.
Okayama, Y., Kawakami, T., 2006. Development, migration, and survival of mast cells. Immunol. Res. 34 (2), 97–115.
Pathak, A., 2018. Modeling and predictions of biphasic mechanosensitive cell migration altered by cell-intrinsic properties and matrix confinement. Phys. Biol. 15 (6), 065001.
Pelham, R.J., Wang, Y.L., 1997. Cell locomotion and focal adhesions are regulated by substrate flexibility. Proc. Natl. Acad. Sci. 94 (25), 13661–13665.
Peyton, S.R., Putnam, A.J., 2005. Extracellular matrix rigidity governs smooth muscle cell motility in a biphasic fashion. J. Cell. Physiol. 204 (1), 198–209.
Prahl, L.S., Stanslaski, M.R., Vargas, P., et al., 2020. Predicting confined 1D cell migration from parameters calibrated to a 2D motor-clutch model. Biophys. J. 118 (7), 1709–1720.
Ribatti, D., 2019. The Mast Cell: A Multifunctional Effector Cell. Springer Nature Switzerland AG.
Saigusa, R., Asano, Y., Yamashita, T., et al., 2018. Systemic sclerosis complicated with localized scleroderma-like lesions induced by Köbner phenomenon. J. Dermatol. Sci. 89 (3), 282–289.
Stroka, K.M., Aranda-Espinoza, H., 2009. Neutrophils display biphasic relationship between migration and substrate stiffness. Cell Motil. Cytoskel. 66 (6), 328–341.
Terada, T., Matsunaga, Y., 2000. Increased mast cells in hepatocellular carcinoma and intrahepatic cholangiocarcinoma. J. Hepatol. 33 (6), 961–966.
Tzvetkova-Chevolleau, T., Stéphanou, A., Fuard, D., et al., 2008. The motility of normal and cancer cells in response to the combined influence of the substrate rigidity and anisotropic microstructure. Biomaterials 29 (10), 1541–1551.
Ulrich, T.A., de Juan Pardo, E.M., Kumar, S., 2009. The mechanical rigidity of the extracellular matrix regulates the structure, motility, and proliferation of glioma cells. Cancer Res. 69 (10), 4167–4174.
Wang, H.W., Tedla, N., Lloyd, A.R., et al., 1998. Mast cell activation and migration to lymph nodes during induction of an immune response in mice. J. Clin. Investig. 102 (8), 1617–1626.
Wang, M., Yang, Y., Han, L., et al., 2020. Effect of three-dimensional ECM stiffness on cancer cell migration through regulating cell volume homeostasis. Biochem. Biophys. Res. Commun. 528 (3), 459–465.
Wells, R.G., Discher, D.E., 2008. Matrix elasticity, cytoskeletal tension, and TGF-β: the insoluble and soluble meet. Sci. Signal. 1 (10), 13.
Wong, J.Y., Velasco, A., Rajagopalan, P., et al., 2003. Directed movement of vascular smooth muscle cells on gradient-compliant hydrogels. Langmuir 19 (5), 1908–1913.
Yang, H.W., Liu, X.Y., Shen, Z.F., et al., 2018. An investigation of the distribution and location of mast cells affected by the stiffness of substrates as a mechanical niche. Int. J. Biol. Sci. 14 (9), 1142.
Yangben, Y., Wang, H., Zhong, L., et al., 2013. Relative rigidity of cell–substrate effects on hepatic and hepatocellular carcinoma cell migration. J. Biomater. Sci.-Polym. Eng. 24 (2), 148–157.
Yeung, T., Georges, P.C., Flanagan, L.A., et al., 2005. Effects of substrate stiffness on cell morphology, cytoskeletal structure, and adhesion. Cell Motil. Cytoskel. 60 (1), 24–34.
Zhang, D., Ding, G., Shen, X., et al., 2008. Role of mast cells in acupuncture effect: a pilot study. Explore 4 (3), 170–177.
Zhong, Y., Ji, B., 2013. Impact of cell shape on cell migration behavior on elastic substrate. Biofabrication 5 (1), 015011.